https://doi.org/10.3311/PPCh.22748

Periodica Polytechnica Chemical Engineering, 67(4), pp. 547–556, 2023

Determining the Quintet Lifetimes in Side-ring Substituted $[Fe(terpy)_2]^{2+}$ Complexes

Andor Vancza[1,2*], Marcell Levente Kapta[1], Mariann Papp[1], György Vankó[1], Tamás Keszthelyi[1]

[1] Wigner Research Centre for Physics, H-1525 Budapest, P.O.B. 49, Hungary
[2] Department of Physical Chemistry and Materials Science, Faculty of Chemical Technology and Biotechnology, Budapest University of Technology and Economics, Műegyetem rkp. 3, H-1111 Budapest, Hungary
* Corresponding author, e-mail: vancza.andor@wigner.hu

Received: 09 June 2023, Accepted: 04 October 2023, Published online: 16 November 2023

Abstract

We previously studied the effect of 4' substitution in iron(II)-bis-terpyridine complexes, showing that the photoexcited high-spin quintet-state is stabilized by electron-donating substituents. In this paper we explore the effects of electron-donating ($X = NH_2$, Cl) and withdrawing ($X = NO_2$) substituents in the 5,5" positions on the stability and lifetime of the quintet-state. We used a simple densitiy-functional theory (DFT) based method that had been proven fairly accurate in the case of 4' substitution to estimate the energy barrier of the quintet-singlet transition and thereby predict the quintet state lifetime. We synthetized the complexes and used ultrafast transient optical absorption spectroscopy to experimentally determine the quintet lifetimes, in order to test the applicability of these quantum-chemistry based predictive methods for these side-ring substitution cases. UV-Visible spectra of the complexes have shown that the metal-to-ligand charge transfer (MLCT) and ligand-localized transitions of these complexes change according to the previous observations. We have shown that in the 5,5" positions, electron withdrawing groups stabilize the quintet state, while donating groups destabilize it. This is in stark contrast to the effects previously observed for the 4' case, and indicates that unlike the latter case, the simple concept of inductive and mesomeric effects may not be adequate to describe the changes due to 5,5" substitution, warranting further study of the area.

Keywords

coordination complexes, iron, substituent effects, spin state transition, molecular engineering, terpyridine, transient absorption spectroscopy, pump-probe spectroscopy

1 Introduction

Transition metal based compounds have long been in the focus of efforts to develop molecular devices for various purposes, such as molecular switches and memory devices [1–5], or catalysts and light-harvesting systems [6–10]. In this respect the main characteristic of these molecules is that, being photoactive compounds, they can be conveniently activated or deactivated with light irradiation. Many of the more advanced compounds studied for these purposes employ 5th and 6th row transition metals, but from an environmental and economical point of view there is certainly a necessity to try and utilize more abundant and less harmful alternatives, such as iron.

Our primary interests are Fe(II)-based coordination complexes with a low-spin (singlet) ground-state at room temperature (see in Scheme 1). These complexes can be switched to a high-spin (quintet) state either thermally or by light irradiation. This state is short-lived, but can become metastable at extremely low temperatures, the phenomenon being referred to as light-induced excited spin-state trapping (LIESST) [11–13]. Similar results at room temperature have not yet been achieved.

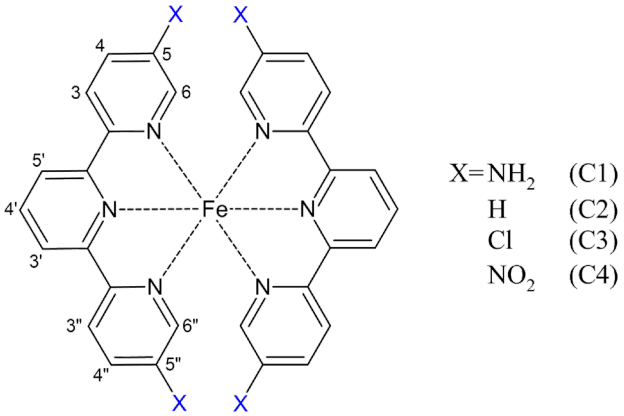

Scheme 1 Schematic structure of the studied complexes

Cite this article as: Vancza, A., Kapta, M. L., Papp, M., Vankó, G., Keszthelyi, T. "Determining the Quintet Lifetimes in Side-ring Substituted $[Fe(terpy)_2]^{2+}$ Complexes", Periodica Polytechnica Chemical Engineering, 67(4), pp. 547–556, 2023. https://doi.org/10.3311/PPCh.22748

Such complexes could be utilized as molecular switches in ultrafast memory devices.

The 2,2';6',2"-terpyridine (terpy) ligand [14, 15] and its derivatives are the main area of interest for our group. It was demonstrated that its complex with Fe(II) can have a very long-lived quintet state below 30 K [16, 17]. To tune the quintet-lifetime at higher temperatures, we explore the effects of various substituents at different positions. By learning more about the effect of these substituents we can come closer to ways to obtain long-lived quintet states at close to room temperatures as well.

Upon photoexcitation with green or blue light the $[Fe(terpy)_2]^{2+}$ complex is promoted to a singlet metal-to-ligand charge transfer (MLCT) state, followed by multi-step relaxation comprised of ultrafast (sub-picosecond) transitions through MLCT and metal-centered (MC) states until the metastable quintet ^{5}MC state is reached. A detailed theoretical study by our group has shown that the dominant relaxation process is the ^{1}MLCT → ^{3}MLCT → ^{3}MC($^3T_{2g}$) → ^{3}MC($^3T_{1g}$) → ^{5}MC route [18]. From this point, the system returns to the singlet ground-state.

We previously studied the effect of electron-withdrawing (EW) and donating (ED) substituents on the quintet-state lifetime of the $[Fe(4'\text{-R-terpy})_2]^{2+}$ system [19] and conducted a rigorous study on the effects of the Cl-substituent at various positions [20]. These studies have confirmed that modifications at positions with *para*-relation to the axial nitrogen (N_{ax}) in the central ring can induce significant changes in the potential-energy surface (PES). ED groups in the 4' position stabilize the quintet state and lengthen its lifetime by increasing the classical energy barrier of the transition, best described along the coordinates of the breathing mode [19], while EW groups shorten it due to their opposite effect [21]. Among the combined Fe–N bond stretchings of the breathing mode, the Fe–N_{ax} bond length is important, because the axial nitrogen is closer to the central Fe^{2+} ion than the equatorial nitrogens (N_{eq}) of the side-rings [15], thus becoming a sensitive descriptor to the stability of the various states of the complex. This effect of substitution upon the energy barrier was shown to originate from the change in the quintet-singlet energy gap.

The subject of the present study is the effect of symmetric substitution in the 5,5" positions of the side-rings. The Cl substituent was previously shown to act in a similar manner in both the 4', and the 5,5" positions, lengthening the quintet lifetime in both cases [20]. However, as Cl is a substituent with a medium-strength −I and a weak +M effect, we have concluded that groups with stronger effects need to be studied as well, since we may expect interesting behavior from these. Therefore, here we study the effects of NO_2 (strong –I and –M effects) and NH_2 (weak –I and strong +M effects) groups in addition to the Cl atom. We synthesized the complexes and followed their photorelaxation using transient optical absorption spectroscopy (TOAS). Based on the calculations and previous experimental results [15, 18, 20], it can be safely assumed that the final relaxation step with lifetimes in the nanosecond range belongs to the quintet-singlet relaxation process in all complexes discussed in this paper. We also provide calculation-based predictions of these lifetimes using simple, but qualitatively accurate methods to further verify their applicability in case of side-ring substitutions. UV-Visible spectroscopy measurements were also performed as the positions of the absorption bands pertaining to the MLCT transitions had previously also been shown to be dependent on the EW/ED effects of the substituent moieties [20].

With this study we aim to broaden our understanding of the connection between the changes in the PES (and consequently the quintet-state lifetime) and the substituent effects. Doing so we can extend our arsenal of methods to eventually be able to tune the excited-state properties of Fe(II)-bis-terpyridine and analogous complexes precisely and accurately according to any specific need, bringing us closer to their application as room-temperature photoactivated molecular devices.

2 Experimental and theoretical methods

2.1 Syntheses of the complexes

2,2':6',2"-terpyridine was purchased from Sigma-Aldrich, the other derivatives were obtained from EVOBlocks Ltd, Budapest. Methanol and acetonitrile were purchased from Molar Chemicals. Toluene, NH_4PF_6, NH_4BF_4, $Fe(BF_4)_2{\cdot}6H_2O$, $FeCl_2{\cdot}4H_2O$, Celite 545, and silica-gel TLC plates were purchased from Sigma-Aldrich.

In all cases TLC test of the final product was performed on a silica gel plate to confirm the absence of side products and contaminations. The eluent used was a 4:1:1 mixture of acetonitrile, methanol, and water saturated for KNO_3. ^{1}H NMR measurements have shown that the products contain significant amounts of solvent in their crystals.

2.1.1 C1: $[Fe(5,5''\text{-di-}NH_2\text{-terpy})_2](BF_4)_2$

2,2':6',2"-terpyridine-5,5"-diamine (0.193 g, 0.733 mmol) was dissolved in 50 ml of acetonitrile. $Fe(BF_4)_2{\cdot}6H_2O$ (0.120 mg, 0.355 mol) was dissolved in 5 ml of water and added to the ligand solution. The reaction mixture was

stirred at room temperature for 4 hours. TLC tests have shown that the mixture contains a small amount of Fe(III) contamination. The reaction mixture was filtered on a G4 fritted funnel with Celite layered on the frit. This process removed the brownish-yellow Fe(III) contamination by adsorbing it on the Celite layer. A TLC test was performed on the filtrate, which confirmed the absence of contamination. The solution was evaporated from the filtrate at 313 K and the solid was dried at 333 K. The products were purplish-red crystals (0.251 g, 0.343 mmol, 96% yield).

^{1}H NMR (400 MHz, Acetonitrile-d3) δ [ppm] 8.41–8.34 (m, 2H), 8.05 (*d*, *J* = 8.6 Hz, 1H), 6.97 (*dd*, *J* = 8.8, 2.5 Hz, 1H), 6.39 (*dd*, *J* = 2.5, 0.5 Hz, 1H).

^{13}C NMR (101 MHz, Acetonitrile-d3) δ 161.1, 148.0, 147.0, 138.9, 137.7, 124.7, 121.8, 119.1.

2.1.2 C2: $[Fe(terpy)_2](BF_4)_2$

The preparation of $[Fe(terpy)_2]Cl_2$ was presented in our previous paper [19]. $[Fe(terpy)_2]Cl_2$ (0.424 g, 0.714 mmol) was dissolved at room temperature in H_2O and NH_4BF_4 was added to the solution in great excess to precipitate $[Fe(terpy)_2](BF_4)_2$. The resulting purple solid was removed from the dispersion by filtration on a G4 glass fritted funnel. The product was washed with water and dissolved from the frit with acetonitrile. The solvent was evaporated at 313 K and the solid dried at 333 K. The products were purple crystals (0.488 g, 0.359 mmol, 98% yield).

^{1}H NMR (400 MHz, Acetonitrile-d3) δ [ppm] 8.92 (*d*, *J* = 8.0 Hz, 2H), 8.68 (*t*, *J* = 8.0 Hz, 1H), 8.48 (*d*, *J* = 8.0 Hz, 2H), 7.88 (m, 2H), 7.07 (m, 4H).

^{13}C NMR (101 MHz, Acetonitrile-d3) δ 161.2 158.7, 154.0, 139.7, 138.9, 128.3, 124.7, 124.6.

2.1.3 C3: $[Fe(5,5''\text{-di-Cl-terpy})_2](PF_6)_2$

The preparation of $[Fe(5,5''Cl\text{-terpy})_2](PF_6)_2$ was presented in our previous paper [20].

^{1}H NMR (400 MHz, Acetonitrile-d3) δ [ppm] 8.90 (*d*, *J* = 8.1 Hz, 2H), 8.70 (*t*, *J* = 8.1 Hz, 1H), 8.41 (*d*, *J* = 8.7 Hz, 2H), 7.92 (*dd*, *J* = 8.7, 2.2 Hz, 2H), 6.88 (*d*, *J* = 2.2 Hz, 2H).

^{13}C NMR (101 MHz, Acetonitrile-d3) δ 160.75, 157.47, 152.89, 139.96, 139.68, 135.52, 125.55, 125.53.

2.1.4 C4: $[Fe(5,5''\text{-di-}NO_2\text{-terpy})_2](BF_4)_2$

5,5''-dinitro-[2,2':6',2''-terpyridine] (0.297 g, 0.920 mmol) was dispersed in 50 ml of acetonitrile. $Fe(BF_4)_2 \cdot 6H_2O$ (0.150 g, 0,444 mmol) was dissolved in 10 ml of methanol, and added to the ligand dispersion. The reaction mixture was stirred at 343 K for 2 hours, and a further 12 hours at room temperature. The reaction mixture was filtered on a G4 fritted funnel. The solution was evaporated from the filtrate at 313 K and the solid was dried at 333 K. The products were blueish-purple crystals (0.315 g, 0.359 mmol, 81% yield).

^{1}H NMR (400 MHz, Acetonitrile-d3) δ [ppm] 9.24 (*d*, *J* = 8.1 Hz, 2H), 8.95 (*t*, *J* = 8.1 Hz, 1H), 8.73 (*d*, *J* = 8.8 Hz, 2H), 8.61 (*dd*, *J* = 8.8, 2.3 Hz, 2H), 7.55 (*d*, *J* = 2.2 Hz, 2H).

^{13}C NMR (101 MHz, Acetonitrile-d3) δ 163.0 160.5, 150.5, 146.6, 140.8, 135.6, 128.6, 125.8.

2.2 Sample characterization

UV-Visible spectra of the complexes were measured with a Jasco V-750 UV-Visible spectrophotometer in acetonitrile solutions with concentrations of 0.02–0.03 mM, in 10 mm optical path-length quartz cuvettes.

^{1}H and ^{13}C NMR spectra were recorded on a Varian NMR System 400 spectrometer in CD_3CN (Sigma-Aldrich) at 298 K. Measurements were performed using an indirect detection Z probe. The chemical shifts are referenced to the residual solvent signal at 1.94 ppm. The ^{1}H NMR spectra of **C2** is consistent with that which Elsbernd and Beattie [22]. measured in D_2O, and the chemical shift values are virtually equal with the ones presented in [23], measured in CD_3CN. The spectrum of **C3** is consistent with that of $[Fe(5,5''\text{-di-Cl-terpy})_2]Cl_2$ in our previous article [20]. **C1** and **C4** are new complexes and have no previously published NMR results available.

2.3 Computational details

For all the densitiy-functional theory (DFT) calculations presented in this work the ORCA 5.0.0 [24–26] quantum chemistry program package was utilized.

For both the low spin and high spin state of the complexes geometry optimization was performed with the B3LYP* functional [27] using the TZVP basis set. B3LYP* is a hybrid functional that contains 15% Hartree-Fock exact exchange contribution and is known to provide satisfactory energies for iron complexes. The RIJCOSX [28, 29] approximation was also employed to reduce computational costs of using the B3LYP* hybrid functional.

Minimum energy crossing points (MECP) were also determined [30] between the aforementioned states. During MECP calculations both the geometry and the energy difference of the states involved were optimized. All the calculations were started from the quintet minimum.

The conductor-like polarizable continuum model (CPCM) [31] implicit solvation method was applied in all the calculations mentioned above.

2.3.1 Calculating the quintet→singlet energy barrier

Previously our group presented a simple, but in most cases adequately accurate method to estimate the quintet state lifetimes of substituted Fe(II)-bis-terpyridine complexes [19]. The method relies on a semiclassical description of the relaxation process, explaining the lifetime to be inversely proportional to the quintet-singlet energy difference (ΔE_{HL}) [32]. With this method we make the assumption that only the energy difference of the quintet and singlet states changes with the substitution, and both the position and the shape of the PES remain that of the base molecule, **C2**. Thus using the potential energy surface previously calculated along the quintet-singlet relaxation coordinate by the very accurate CASPT2 method for **C2** [14], and shifting it according to the ΔE_{HL} calculated by DFT the crossing point between these surfaces can be numerically determined. The difference between the crossing point and the quintet-state energy is the estimate of the classical energy barrier $\left(\Delta E_X^{\ddagger}\right)$ for the quintet-singlet relaxation, which at room temperature can be used to estimate the quintet-state lifetime [19]. For comparison, MECP calculations [30] were performed as well to determine the barrier height $\left(\Delta E_{\mathrm{MECP}}^{\ddagger}\right)$. Fig. 1 schematically displays the relationship between the quintet-singlet energy difference and the height of the semiclassical barrier for the quintet-singlet transition. The ΔE_{HL} of Complex A is higher than that of Complex B, resulting in a lower barrier height and shorter lifetime for the former.

To calculate the lifetime of the quintet→singlet relaxation, we use the Arrhenius equation, employing the barrier heights as the activation energy needed for the process.

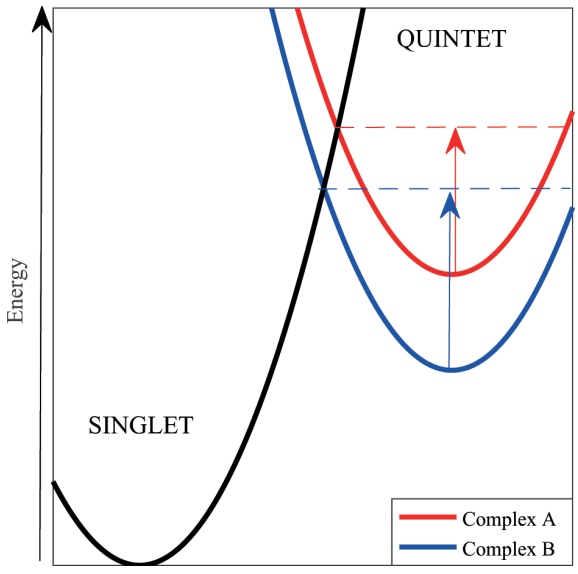

Fig. 1 Quintet-singlet energy differences and their effect on the barrier heights

With the assumption that the pre-exponential factors differ only negligibly for the complexes discussed, Eq. (1) can be used to calculate the lifetime of any complex relative to the base molecule, **C2**:

$$\frac{\tau_i}{\tau_{C2}} = \exp\left(\frac{\Delta E_i^{\ddagger} - \Delta E_{C2}^{\ddagger}}{kT}\right). \tag{1}$$

τ_i, $\Delta E_i^{\ddagger}$ and τ_{C2}, $\Delta E_{C2}^{\ddagger}$ are the lifetime and calculated barrier height of a selected complex and **C2**, respectively. k is the Boltzmann-constant and T is the absolute temperature.

2.4 Transient optical absorption spectroscopy

Femtosecond transient absorption measurements were carried out on our home-built spectrometer. The measurement setup is shown in Scheme 2. The laser is a Spectra Physics Solstice Ace Ti:Sapphire amplifier which produces 35 fs pulses at 1 kHz repetition rate with a central wavelength of 800 nm. 700 mW of the laser output power is utilized for the spectroscopy setup. 90% of the beam is chopped at 500 Hz, delayed with a linear translation stage (Aerotech PRO225LM), and subsequently frequency-doubled in a β-barium-borate (BBO) crystal to produce the 400 nm central wavelength pump beam. The excitation power is fine-tuned using a continuously variable neutral-density filter. The energy at the sample position was set within the range of 0.5–4 μJ depending on the intensity of the transient signal observed. A fraction of the other 10% energy is used for white-light supercontinuum (WLC) generation in a sapphire crystal. This produces a probe beam with a 430–750 nm effective wavelength range. Considering both pump and probe beams at sample. position, the temporal width of the instrument response function is estimated as ~70 fs over the entire spectrum.

The probe beam is split before the sample and registered shot-to-shot using CCD detectors. One beam interacts with the sample and is used for measurement (signal beam). The second (reference) beam reaches the sensor unobstructed and is used to correct for fluctuations in the supercontinuum. A photodiode is used to monitor the intensity fluctuation of the pump beam, which is used to perform shot-to-shot correction. For each delay position 1000 data points were measured, which were averaged during data pre-processing. Multiple scans (usually 5 to 9) were taken during each measurement, which were averaged during data processing. Pump-only data points were taken to allow accurate baseline correction for each scan. The measurement control software, the pre-processing and the analysis scripts were in-house written.

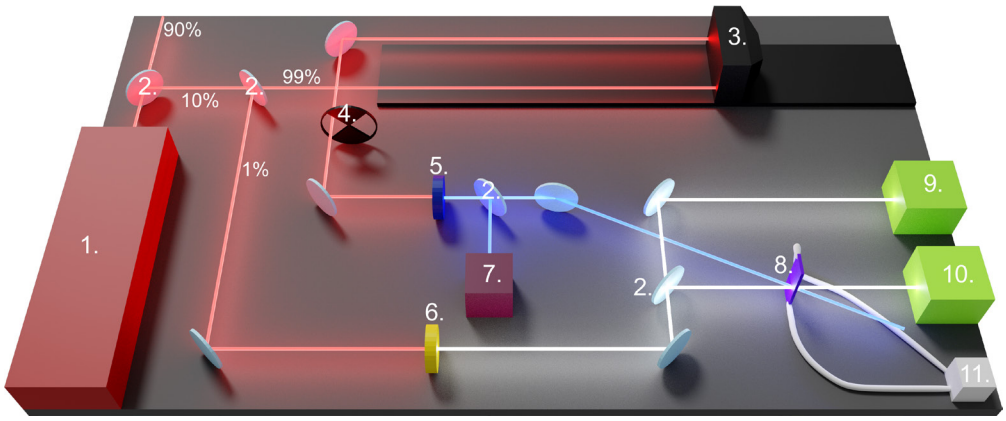

Scheme 2 Schematic representation of the TOAS setup. 1: laser source; 2: beamsplitters; 3: delay stage; 4: chopper; 5: BBO crystal; 6: WLC generation in a sapphire crystal; 7: photodiode; 8: quartz flow cell; 9: reference detector; 10: sample detector; 11: peristaltic pump

The sample solution was circulated in a quartz flow cell with 0.5 mm optical path and 0.2 mm thick walls during the measurement. Measurements were carried out on acetonitrile solutions of the complexes with concentrations pertaining to 0.7 optical density (OD) peak absorbance in the path length.

The circulation was used to avoid sample degradation due to the long-term exposure to the laser beam. The thinned walls reduce the intensity and simplify the temporal structure of the coherent artifact (CA) [33, 34]. Since the topic of this paper is the quintet-state lifetime – which for substituted Fe(II)-terpyridine complexes we have shown to be in the order of nanoseconds [19, 20] – we utilized the full available delay stage length, allowing for measurement up to 10 ns of delay time. The step size used was 6.6 ps up until 60 ps of delay, where it was increased to 66 ps for the rest of the path length. The group-velocity dispersion (GVD) and the coherent artifact can be disregarded for the quintet-lifetime determination. The latter occurs in the first 100 fs, and is skipped entirely during these measurements, while the former is not relevant when using a narrow wavelength range for fitting (see Section 3.2.1).

2.4.1 Data processing and corrections

During and after measurement multiple types of corrections and data-manipulation are carried out to ensure the accuracy of the data:

- **Baseline correction:** before and after each scan pump-only ("dark") data with the probe beam blocked are measured on the whole wavelength range to serve as a baseline. This correction is made on the fly during measurement.
- **Intensity-fluctuations:** a separate, "reference" detector is used to measure the spectrum of the white-light continuum for each laser shot, which is used to correct for its temporal fluctuations in the following manner:

$$\Delta A = -\lg\left(\frac{I_S^* / I_S}{I_R^* / I_R}\right). \quad (2)$$

ΔA is the differential absorbance, I_S and I_R are the measured intensities at the sample and reference detectors respectively, while the star represents the pumped pulses. A photodiode is used to monitor the intensity of the pump beam also on a shot-by-shot basis, which during pre-processing is normalized to 1 by division with its mean and used as a correction factor for the fluctuation of the pump intensity.

- **Drift-correction:** the laser beam has imperfect beam-pointing stability, which can be attributed to multiple causes, including thermal expansion/contraction of materials, vibrations, the movement of the delay stage, and even internal factors from the laser source itself. This poses the problem that during measurement the pump and probe beams may drift apart at the sample position, reducing the overlap area, which in turn causes a loss of transient absorbance. The sources of the drift are difficult to completely counteract, for which reason we use a follow-up correction by measuring additional data points before and after each scan at ~400 ps delay position. These points are fitted with a linear function for each scan separately, and these functions are used to correct for the minor, systematic changes in the overlap.

3 Results and discussion

3.1 UV-Visible spectra

Our previous studies of modified Fe(II)-bis-terpyridine complexes have shown that the change in the molecular orbital energies due to the ED/EW nature of the substituent

is significant enough to cause noticeable red/blue shifts in the UV-Visible spectra for multiple peaks. Fig. 2 shows the measured spectra and Table 1 displays the positions of the bands discussed below.

The visible region comprises of $t_{2g} \rightarrow \pi^*$ MLCT transitions (the former being the HOMO and the latter the LUMO, dominantly made of the side-ring π^*-orbitals) [20, 35]. In the case of the Cl substituent these transitions were found to be mostly insensitive of substitution in the 5(5") position due to the HOMO and LUMO orbital energies shifting to lower energies in parallel to each other with the addition of one and two Cl substituents [20]. This is exactly what we can see if we compare the spectra of **C2** and **C3** in Fig. 2. The MLCT peak belonging to **C4** is shifted towards longer wavelengths and shows significant broadening. The peak belonging to **C1** is very similar to **C3,** with a significant increase in the intensity at the 460 and 390 nm peaks. A minor blue shift is also noticeable. However, with the inclusion of **C3** and **C2** the four complexes seem to show no clear trend in relation with the EW/ED strength of the substituents, which is also in line with our previous observations from the examination of the Cl-substitution and the spectra of various 4' substituted complexes [19].

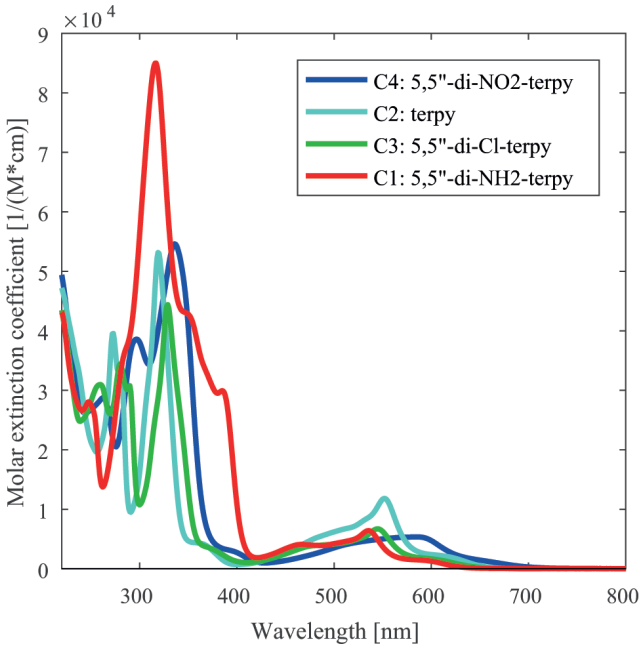

Fig. 2 Experimental UV-Visible spectra of the complexes in acetonitrile solutions

Table 1 Peaks of the UV-Visible absorptions bands belonging to the MLCT and $\pi \rightarrow \pi^*$ transitions

Complex	MLCT (nm)	$\pi \rightarrow \pi^*$ (nm)
C1 (5,5"-di-NH_2-terpy)	535	317
C2 (terpy)	552	319
C3 (5,5"-di-Cl-terpy)	545	329
C4 (5,5"-di-NO_2-terpy)	585	336

In the UV-region the peak with the most significant shift due to substitution is the one situated between 300–360 nm. Our rigorous study of the 5-Cl substitutions previously has shown that, in contrast to an earlier interpretation in case of similar complexes, these transitions are not MLCT, but involve $\pi \rightarrow \pi^*$ transitions, between ligand orbitals that are strongly mixed with the $3d_{xy}$, or the $3d_{yz}$ and $3d_{xz}$ orbitals of the iron. The energies of the π^* orbitals decrease with the addition of Cl substituents in the 5(5")-position, while those of the π orbitals remain unaffected, resulting in a red shift of the corresponding peak in the spectrum [20]. Here we can see this reinforced when also taking **C4** into consideration, where the significant increase of the −I effect shifts the peak further to the red. The fact that **C1** shows no significant blue shift compared to **C2** is somewhat surprising but this can be attributed to the significantly different peak structure observable in the UV-region compared to the other complexes. The same can be said about the MLCT band of **C4** and therefore we conclude that calculated UV-Visible spectra are needed to be able to discern the observed effects more in-depth, in case of both the MLCT and $\pi \rightarrow \pi^*$ bands.

3.2 Experimental determination of the quintet-state lifetime

To determine the quintet lifetime of the four complexes we carried out TOAS measurements in acetonitrile solutions. The distribution of time delay steps described in Section 2.4 was chosen instead of the full precision (70 fs) allowed by our setup, because this allows a simple, yet proven to be accurate data analysis method whereas a more detailed measurement takes significantly more time and requires more rigorous data pre-processing and global analysis to determine the quintet lifetime. According to our experience with nanosecond-scale lifetimes the additional precision that it may provide is usually negligible (strictly in case of the quintet lifetime). Granted, this choice of time delay steps provides no insight to the early events of the relaxation process. For these, more accurate measurements and extensive global and target analysis [36] are being carried out currently.

3.2.1 Data analysis

Figs. 3 and 4 shows the evolution of the differential-absorbance spectrum with the increase of the time delay for the newly synthetized complexes. The negative values are

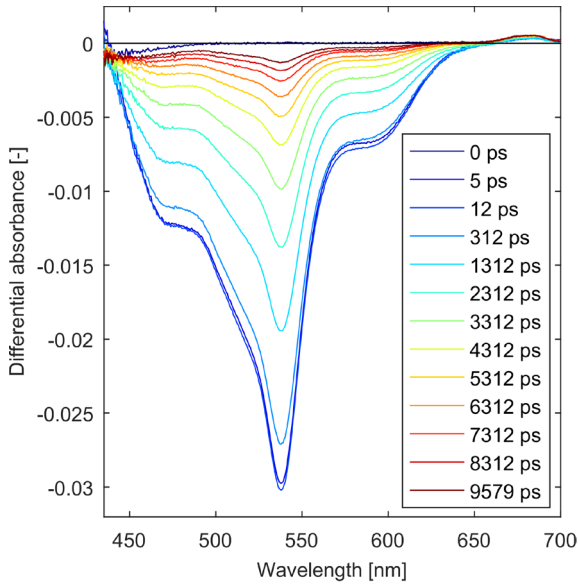

Fig. 3 Transient spectra of **C1** at different time-delays

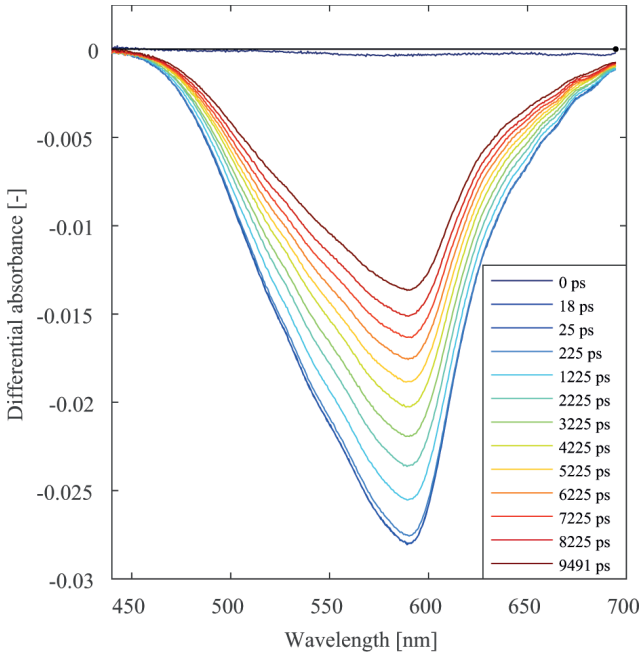

Fig. 4 Transient spectra of **C4** at different time-delays

a result of the ground state bleach (GSB), occurring due to the peak pertaining to the MLCT transition missing in the quintet state. This large GSB signal allows a simple determination of the quintet lifetime.

Based on extensive relaxation-dynamics calculations on the parent molecule [18], we can assume that only the quintet→singlet relaxation process happens on the nanosecond scale, and all preceding transitions are complete in the first tens of picoseconds. Based on this, a single exponential decay adequately describes the quintet→singlet relaxation, however some other factors are needed to be considered. For this reason, the fitting equation is a convolution of said exponential decay, a Heaviside step function to model the excitation, and a Gaussian function to model the instrument response function (IRF) [37].

A 100 fs full width at half maximum (FWHM) was fixed for the Gaussian as the delay steps employed do not allow accurate fitting of the IRF. The fitting was done at the GSB maximum since the disappearance of the GSB signal is tied to the quintet→singlet transition. For each complex, a bandwidth of 3.5 nm (6 channels) was averaged and used for the fitting process. The results can be seen in Fig. 5.

Comparing **C2** and **C3** the same relation can be seen as reported previously in H_2O [20]. The Cl substituent causes a significant increase in the quintet lifetime (*ca.* 50%). Comparing **C4** and **C1** to the base molecule (**C2**), the lifetime is almost doubled due to the NO_2 substituent and shows a decrease by 1.5 ns (38%) due to the NH_2 group.

3.3 Discussion of the results

Previously we have shown that substitution with EW groups in the 4' position causes a shortening of the quintet lifetime, while ED groups stabilize the high-spin state. The quintet state is most sensitive to the substitution on the central ring, and especially in this position. The reason for this is that in the quintet state the orbitals get populated which are very susceptible to the axial modification, especially the changes in the Fe-N_{ax} bond length [15, 19].

In the 4' position both the inductive and resonance effects can significantly affect the lifetime. Given that all

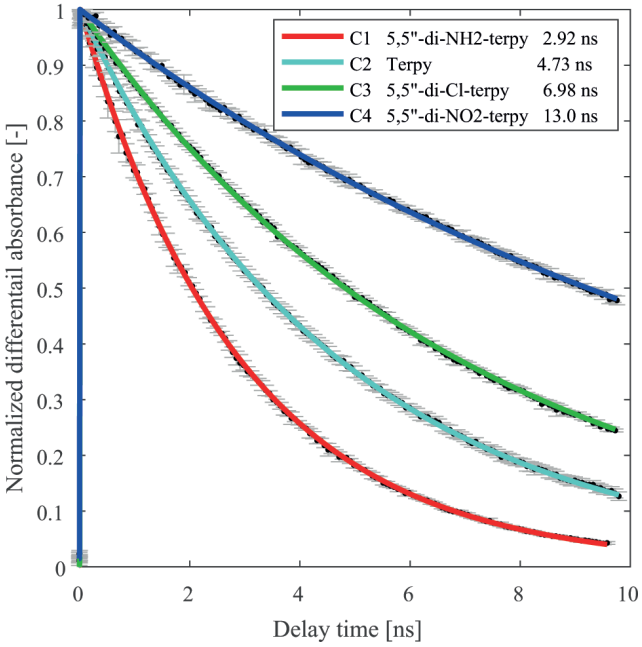

Fig. 5 Quintet lifetime fitting of the complexes discussed, measured in acetonitrile solutions at 295 K

substituents discussed in [19] have a –I effect, the deciding factor is the ratio of their –I and –M/+M strength, the latter very pronounced in the 4' position, being a *para*-position relative to N_{ax}. At first glance the results seen here conflict with these previous observations, but it is important to consider that in the 5 position these effects work differently. Since all substituents discussed in this paper have a –I effect (although of varying strength), the main differentiating factor is once again resonance. The –I effect is expected to decrease the N_{eq} electron-density similarly to the Cl substituent [20], while the resonance effects should be negligible in this position, given that the position 5 and N_{eq} are in *meta*-relation. This means that the –I strengths should be the deciding factor for changes related to the side rings (cf. the discussion of the $\pi \rightarrow \pi^*$ absorption bands above).

The calculated and measured lifetimes are shown in Table 2. As we previously discussed, changes in the quintet state lifetime due to substitution are primarily attributed to the effects of the substituent on the central ring (specifically N_{ax}) [19–21]. Due to their distance the inductive effects of substituents in the 5 and 5" positions are not expected to affect N_{ax}. On the other hand, resonance effects can reach it, the central ring being in *para*-position to the substituent and N_{ax} being in *ortho*-relation with side-rings. However, the NH_2 group unexpectedly causes a shorter quintet lifetime while the NO_2 group lengthens it, which shows changes in the opposite direction from what we would conclude based on our previous observations [20].

Comparing the measured and calculated lifetimes we can see that there is good agreement between the two, even on the quantitative level, with only **C2** being the case where both calculation methods overestimate the increase in the quintet lifetime. Our previous conclusion regarding the PES-crossing and MECP methods, that although the former uses a very simplified concept it produces just as good or even better results than the latter, is reinforced with these new results. The minor quantitative disagreements with the experiments can be easily attributed to the general limitations of the calculations and the assumption that the shape of the PES does not change with the substitution compared to the base molecule. As the shifts in the UV-Vis spectral bands of the ground state occur in line with the expectations from previous observations, we can presume that the EW/ED effects apply as expected. However, the results strongly indicate that while the simple ED/EW explanation may not sufficiently describe the changes in the electronic structure in more complicated cases, the predictions based on the inverse energy gap rule [17] are still very accurate.

4 Conclusion

Extending our previous work on modified terpyridine ligands we synthetized and characterized two new $[Fe(5,5"\text{-di-X-terpy})_2]^{2+}$ complexes. We performed TOAS measurements to determine their quintet-state lifetime with the intention to further understand the relation between EW/ED effects and the stability of the quintet state. We have shown that strong substituent effects originating from the 5,5" positions on the side-rings cause opposite changes in the stability and lifetime of the high-spin quintet-state compared to the 4' position. EW effects here significantly increase the lifetime, while ED effects shorten them. However these changes were accurately predicted by our calculations based on the inverse energy gap law.

Therefore, the general tendency of quintet-state lifetime vs. substituent effects observed for substituents in the 4' position cannot be extrapolated to the $[Fe(5,5"\text{-di-X-terpy})_2]^{2+}$ system. Another important fact to note is that the rigorous analysis of the effects of Cl-substitution was not enough to draw conclusion regarding the side-ring substitutions, since it suggested a similar tendency as the 4' case. Further effort is required both in experimental work and calculations to provide a definite answer to the questions posed by these results, which is currently in progress. Extending our investigations to include the early events of the relaxation process *via* more detailed TOAS measurements and global and target analysis [36] is the important next step. In addition, extensive calculations are being carried out to understand the dynamics of the complexes in question.

Table 2 Calculated quintet-singlet energy differences, barrier heights and lifetimes, and experimental lifetimes of the discussed complexes. All experimental lifetimes have a standard error of less than 30 ps. Data marked with the "*" symbol are from [20]

Complex	ΔE_{HL} (meV)	$\Delta E_X^{\ddagger}$ (meV)	$\Delta E_{MECP}^{\ddagger}$ (meV)	Relative lifetime			Experimental absolute lifetime (ns) (acetonitrile, 295 K)
				X	MECP	Experimental	
C1 (5,5"-di-NH2-terpy)	522	100	105	0.78	0.53	0.63	2.92
C2 (terpy)	505*	103*	118*	1	1	1	4.73
C3 (5,5"-di-Cl-terpy)	450*	122*	144*	2.1	2.9	1.5	6.98
C4 (5,5"-di-NO_2-terpy)	432	128	150	2.65	2.96	2.8	13.0

Acknowledgement

This project was supported by the National Research, Development and Innovation Fund of Hungary (NKFIH) under project number 2018-1.2.1-NKP-2018-00012. We thank Dr. Attila Domján and Dr. Gábor Turczel (both at the Research Centre for Natural Sciences, Budapest) for the NMR measurements, Dr. Gábor Bazsó (Wigner RCP) for constructing the TOAS instrument and Dr. László Varga (EVOBlocks Ltd, Budapest) for the syntheses of the ligands and Levente Zemlényi for preparing Scheme 2.

References

[1] Venkataramani, S., Jana, U., Dommaschk, M., Sönnichsen, F. D., Tuczek, F., Herges, R. "Magnetic Bistability of Molecules in Homogeneous Solution at Room Temperature", Science, 331(6016), pp. 445–448, 2011. https://doi.org/10.1126/science.1201180

[2] Kahn, O., Martinez, C. J. "Spin-Transition Polymers: From Molecular Materials Toward Memory Devices", Science, 279(5347), pp. 44–48, 1998. https://doi.org/10.1126/science.279.5347.44

[3] Bousseksou, A., Molnár, G., Matouzenko, G. "Switching of Molecular Spin States in Inorganic Complexes by Temperature, Pressure, Magnetic Field and Light: Towards Molecular Devices", European Journal of Inorganic Chemistry, 2004(22), pp. 4353–4369, 2004. https://doi.org/10.1002/ejic.200400571

[4] Sato, O., Tao, J., Zhang, Y.-Z. "Control of magnetic properties through external stimuli", Angewandte Chemie International Edition, 46(13), pp. 2152–2187, 2007. https://doi.org/10.1002/anie.200602205

[5] Dey, B., Mehta, S., Mondal, A., Cirera, J., Colacio, E., Chandrasekhar, V. "Push and Pull Effect of Methoxy and Nitro Groups Modifies the Spin-State Switching Temperature in Fe(III) Complexes", ACS Omega, 7(43), pp. 39268–39279, 2022. https://doi.org/10.1021/acsomega.2c05380

[6] Agarwal, J., Fujita, E., Schaefer, H. F., Muckerman, J. T. "Mechanisms for CO Production from CO_2 Using Reduced Rhenium Tricarbonyl Catalysts", Journal of the American Chemical Society, 134(11), pp. 5180–5186, 2012. https://doi.org/10.1021/ja2105834

[7] Schneider, T. W., Hren, M. T., Ertem, M. Z., Angeles-Boza, A. M. "$[Ru^{II}(tpy)(bpy)Cl]^{+}$-Catalyzed reduction of carbon dioxide. Mechanistic insights by carbon-13 kinetic isotope effects", Chemical Communications, 54(61), pp. 8518–8521, 2018. https://doi.org/10.1039/C8CC03009J

[8] Lewandowska-Andralojc, A., Polyansky, D. E., Zong, R., Thummel, R. P., Fujita, E. "Enabling light-driven water oxidation *via* a low-energy Ru^{IV}=O intermediate", Physical Chemistry Chemical Physics, 15(33), pp. 14058–14068, 2013. https://doi.org/10.1039/c3cp52038b

[9] Lakadamyali, F., Reisner, E. "Photocatalytic H_2 evolution from neutral water with a molecular cobalt catalyst on a dye-sensitised TiO_2 nanoparticle", Chemical Communications, 47(6), pp. 1695–1697, 2011. https://doi.org/10.1039/c0cc04658b

[10] Arias-Rotondo, D. M., McCusker, J. K. "The photophysics of photoredox catalysis: a roadmap for catalyst design", Chemical Society Reviews, 45(21), pp. 5803–5820, 2016. https://doi.org/10.1039/C6CS00526H

[11] Létard, J.-F. "Photomagnetism of iron(II) spin crossover complexes—the *T*(LIESST) approach", Journal of Materials Chemistry, 16(26), pp. 2550–2559, 2006. https://doi.org/10.1039/B603473J

[12] Hauser, A. "Light-Induced Spin Crossover and the High-Spin→Low-Spin Relaxation", In: Gütlich, P., Goodwin, H. A. (eds.) Spin Crossover in Transition Metal Compounds II, Springer, 2004, pp. 155–198. ISBN 978-3-540-40396-8 https://doi.org/10.1007/b95416

[13] Decurtins, S., Gutlich, P., Hasselbach, K. M., Hauser, A., Spiering, H. "Light-Induced Excited-Spin-State Trapping in Iron(II) Spin-Crossover Systems. Optical Spectroscopic and Magnetic Susceptibility Study", Inorganic Chemistry, 24(14), pp. 2174–2178, 1985. https://doi.org/10.1021/ic00208a013

[14] Pápai, M., Vankó, G., de Graaf, C., Rozgonyi, T. "Theoretical Investigation of the Electronic Structure of Fe(II) Complexes at Spin-State Transitions", Journal of Chemical Theory and Computation, 9(1), pp. 509–519, 2013. https://doi.org/10.1021/ct300932n

[15] Vankó, G., Bordage, A., Pápai, M., Haldrup, K., Glatzel, P., March, A. M., Doumy, G., Britz, A., Galler, A., Assefa, T., Cabaret, D., … Gawelda, W. "Detailed Characterization of a Nanosecond-Lived Excited State: X-ray and Theoretical Investigation of the Quintet State in Photoexcited $[Fe(terpy)_2]^{2+}$", The Journal of Physical Chemistry C, 119(11), pp. 5888–5902, 2015. https://doi.org/10.1021/acs.jpcc.5b00557

[16] Renz, F., Oshio, H., Ksenofontov, V., Waldeck, M., Spiering, H., Gütlich, P. "Strong Field Iron(II) Complex Converted by Light into a Long-Lived High-Spin State", Angewandte Chemie International Edition, 39(20), pp. 3699–3700, 2000. https://doi.org/10.1002/1521-3773(20001016)39:20<3699::AID-ANIE3699>3.0.CO;2-Z

[17] Hauser, A., Enachescu, C., Daku, M. L., Vargas, A., Amstutz, N. "Low-temperature lifetimes of metastable high-spin states in spin-crossover and in low-spin iron(II) compounds: The rule and exceptions to the rule", Coordination Chemistry Reviews, 250(13–14), pp. 1642–1652, 2006. https://doi.org/10.1016/j.ccr.2005.12.006

[18] Rozgonyi, T., Vankó, G., Pápai, M. "Branching mechanism of photoswitching in an Fe(II) polypyridyl complex explained by full singlet-triplet-quintet dynamics", Communications Chemistry, 6(1), 7, 2023. https://doi.org/10.1038/s42004-022-00796-z

[19] Sárosiné Szemes, D., Keszthelyi, T., Papp, M., Varga, L., Vankó, G. "Quantum-chemistry-aided ligand engineering for potential molecular switches: changing barriers to tune excited state lifetimes", Chemical Communications, 56(79), pp. 11831–11834, 2020. https://doi.org/10.1039/D0CC04467A

[20] Papp, M., Keszthelyi, T., Vancza, A., Bajnóczi, É. G., Kováts, É., Németh, Z., Bogdán, C., Bazsó, G., Rozgonyi, T., Vankó, G. "Molecular Engineering to Tune Functionality: The Case of Cl-Substituted $[Fe(terpy)_2]^{2+}$", Inorganic Chemistry, 62(16), pp. 6397–6410, 2023.
https://doi.org/10.1021/acs.inorgchem.3c00271

[21] Kershaw Cook, L. J., Kulmaczewski, R., Mohammed, R., Dudley, S., Barrett, S. A., Little, M. A., Deeth, R. J., Halcrow, M. A. "A Unified Treatment of the Relationship Between Ligand Substituents and Spin State in a Family of Iron(II) Complexes", Angewandte Chemie International Edition, 55(13), pp. 4327–4331, 2016.
https://doi.org/10.1002/anie.201600165

[22] Elsbernd, H., Beattie, J. K. "The NMR spectra of terpyridine and the bis-terpyridine complexes of cobalt(III) and iron(II)", Journal of Inorganic and Nuclear Chemistry, 34(2), pp. 771–774, 1972.
https://doi.org/10.1016/0022-1902(72)80463-9

[23] Pazderski, L., Pawlak, T., Sitkowski, J., Kozerski, L., Szlyk, E. "^{1}H, ^{13}C, ^{15}N NMR coordination shifts in Fe(II), Ru(II) and Os(II) cationic complexes with 2,2':6',2"-terpyridine", Magnetic Resonance in Chemistry, 49(5), pp. 237–241, 2011.
https://doi.org/10.1002/mrc.2739

[24] Neese, F. "The ORCA program system", WIREs Computational Molecular Science, 2(1), pp. 73–78, 2012.
https://doi.org/10.1002/wcms.81

[25] Neese, F. "Software update: the ORCA program system, version 4.0", WIREs Computational Molecular Science, 8(1), e1327, 2018.
https://doi.org/10.1002/wcms.1327

[26] Neese, F., Wennmohs, F., Becker, U., Riplinger, C. "The ORCA quantum chemistry program package", The Journal of Chemical Physics, 152, 224108, 2020.
https://doi.org/10.1063/5.0004608

[27] Reiher, M., Salomon, O., Hess, B. A. "Reparameterization of hybrid functionals based on energy differences of states of different multiplicity", Theoretical Chemistry Accounts, 107(1), pp. 48–55, 2001.
https://doi.org/10.1007/s00214-001-0300-3

[28] Neese, F., Wennmohs, F., Hansen, A., Becker, U. "Efficient, approximate and parallel Hartree-Fock and hybrid DFT calculations. A "chain-of-spheres" algorithm for the Hartree-Fock exchange", Chemical Physics, 356(1–3), pp. 98–109, 2009.
https://doi.org/10.1016/j.chemphys.2008.10.036

[29] Izsák, R., Neese, F. "An overlap fitted chain of spheres exchange method", The Journal of Chemical Physics, 135(14), 144105, 2011.
https://doi.org/10.1063/1.3646921

[30] Harvey, J. N., Aschi, M., Schwarz, H., Koch, W. "The singlet and triplet states of phenyl cation. A hybrid approach for locating minimum energy crossing points between non-interacting potential energy surfaces", Theoretical Chemistry Accounts, 99(2), pp. 95–99, 1998.
https://doi.org/10.1007/s002140050309

[31] Barone, V., Cossi, M. "Quantum Calculation of Molecular Energies and Energy Gradients in Solution by a Conductor Solvent Model", The Journal of Physical Chemistry A, 102(11), pp. 1995–2001, 1998.
https://doi.org/10.1021/jp9716997

[32] Hauser, A., Vef, A., Adler, P. "Intersystem crossing dynamics in Fe(II) coordination compounds", The Journal of Chemical Physics, 95(12), pp. 8710–8717, 1991.
https://doi.org/10.1063/1.461255

[33] Lorenc, M., Ziolek, M., Naskrecki, R., Karolczak, J., Kubicki, J., Maciejewski, A. "Artifacts in femtosecond transient absorption spectroscopy", Applied Physics B, 74(1), pp. 19–27, 2002.
https://doi.org/10.1007/s003400100750

[34] Rasmusson, M., Tarnovsky, A. N., Åkesson, E., Sundström, V. "On the use of two-photon absorption for determination of femtosecond pump–probe cross-correlation functions", Chemical Physics Letters, 335(3–4), pp. 201–208, 2001.
https://doi.org/10.1016/S0009-2614(01)00057-4

[35] Ashley, D. C., Jakubikova, E. "Tuning the Redox Potentials and Ligand Field Strength of Fe(II) Polypyridines: The Dual π-Donor and π-Acceptor Character of Bipyridine", Inorganic Chemistry, 57(16), pp. 9907–9917, 2018.
https://doi.org/10.1021/acs.inorgchem.8b01002

[36] van Stokkum, I. H. M., Larsen, D. S., van Grondelle, R. "Global and target analysis of time-resolved spectra", Biochimica et Biophysica Acta (BBA) - Bioenergetics, 1657(2–3), pp. 82–104, 2004.
https://doi.org/10.1016/j.bbabio.2004.04.011

[37] Haldrup, K., Harlang, T., Christensen, M., Dohn, A., van Driel, T. B., Kjær, K. S., Harrit, N., Vibenholt, J., Guerin, L., Wulff, M., Nielsen, M. M. "Bond Shortening (1.4 Å) in the Singlet and Triplet Excited States of $[Ir_2(dimen)_4]^{2+}$ in Solution Determined by Time-Resolved X-ray Scattering", Inorganic Chemistry, 50(19), pp. 9329–9336, 2011.
https://doi.org/10.1021/ic2006875